

Sterile Neutrino Search Using China Advanced Research Reactor

Gang Guo,¹ Fang Han,¹ Xiangdong Ji,¹ Jianglai Liu,^{1,*} Zhaoxu Xi,¹ and Huanqiao Zhang²

¹*INPAC, Department of Physics and Shanghai Key Laboratory for Particle Physics and Cosmology, Shanghai Jiao Tong University, Shanghai, China*

²*China Institute of Atomic Energy, Beijing, China*

(Dated: April 14, 2021)

Abstract

We study the feasibility of a sterile neutrino search at the China Advanced Research Reactor by measuring $\bar{\nu}_e$ survival probability with a baseline of less than 15 m. Both hydrogen and deuteron have been considered as potential targets. The sensitivity to sterile-to-regular neutrino mixing is investigated under the “3(active)+1(sterile)” framework. We find that the mixing parameter $\sin^2(2\theta_{14})$ can be severely constrained by such measurement if the mass square difference Δm_{14}^2 is of the order of ~ 1 eV².

PACS numbers: 14.60.Pq, 25.30.Pt, 28.41.-i

arXiv:1303.0607v2 [physics.ins-det] 18 Jun 2013

*Electronic address: jianglai.liu@sjtu.edu.cn; Corresponding author

I. INTRODUCTION

Neutrino flavor mixing and oscillation, a direct consequence of non-zero neutrino masses, are well established by experimental data [1]. Most of the experimental data to date, including the recent discovery of θ_{13} [2–4] at nuclear reactors, can be described under the 3-flavor mixing framework [1].

Beyond the standard 3-flavor model, sterile neutrinos are postulated as a special type of (heavy) neutrinos that do not interact electromagnetically, weakly, or strongly, hence the name "sterile". Since 90's in the last century, there have been several neutrino oscillation experiments [5–8] which seemed to detect anomalies beyond the 3-flavor mixing. Quite recently, after a re-evaluation of the nuclear reactor flux prediction [9, 10], a global deficit (2-3 σ level) is emerging in the measured flux from all short baseline reactor neutrino experiments [11]. Global fits under "3(active)+1(sterile)" (or "3+1" in short) framework favor a sizable $\sin^2 2\theta_{14} \sim 0.1$ and a mass splitting Δm_{14}^2 ranging from 1 eV² and above (see, e.g. [12, 13]).

Although somewhat non-standard, sterile neutrinos appear to be the simplest explanation of existing experimental anomalies. They are also candidates for warm or cold dark matter under many theoretical models [14].

Numbers of experiments are underway worldwide to search for normal-to-sterile neutrino oscillations [15], including several projects at nuclear reactors. In this paper, we evaluate the feasibility of carrying out a short baseline neutrino experiment using the upcoming state-of-art China Advanced Research Reactor (CARR) reactor [16] with a thermal power of $\sim 60 \text{ MW}_{th}$.

II. STERILE NEUTRINO SEARCH AT CARR

As will be demonstrated below, to search for eV-scale sterile neutrinos via reactor neutrinos (a few MeV in energy) disappearance, short baseline ($< 15 \text{ m}$) is needed to have sufficient sensitivity. Due to safety regulations, it is nearly impossible to place the detector so close to commercial reactors ($\sim \text{GW}_{th}$). In addition, the core size ($\sim 3 \text{ meter}$) introduces smearing effects to the oscillation signal [17]. Compact research reactors ($\sim 0.1 \text{ GW}_{th}$), on the other hand, are more advantageous in these regards (with a cost of lower neutrino flux

from the core).

A. CARR experimental site

China Advanced Research Reactor (CARR), constructed at the China Institute of Atomic Energy in Beijing, China, is a tank-in-pool, inverse neutron trap type, light water cooled, heavy water reflected, multi-purpose research reactor [16]. The reactor body is immersed in a water pool with 16 m in depth and the core is located 12 m below the pool water surface. The reactor core is about 0.8 m in height and 0.4 m in diameter. CARR takes $\text{U}_3\text{Si}_2\text{-Al}$ as the fuel meat, with a 20% enrichment of ^{235}U in weight. With a thermal power of 60 MW, the maximum output thermal neutron flux is about $1.0 \times 10^{15}\text{n/cm}^2/\text{s}$.

CARR was designed as a general-purpose thermal neutron facility for material and biological researches, as well as for isotopic production/enrichment. At present, there are 9 horizontal and 21 vertical beam lines coupled to user equipments. On the ground level of the experimental hall (where horizontal beam lines are), the center of the reactor core is 120 cm above the floor. The outer diameter of the concrete shielding structure is 5.0 m. With this geometry, the closest radial location for a neutrino detector is about 7 m from the core.

B. Neutrino flux and spectrum at CARR

Nuclear reactor is a very intense source of neutrinos. Pure electron antineutrinos $\bar{\nu}_e$ s are produced via β -decay of fission fragments. For a 1 GW_{th} reactor, there are approximately 2×10^{20} $\bar{\nu}_e$ s emitted per second.

Fission nuclei are dominated by 4 isotopes, ^{235}U , ^{238}U , ^{239}Pu , and ^{241}Pu , while other isotopes contribute less than 0.1%. Direct theoretical calculation of the neutrino flux and energy spectrum bare large uncertainties (at the level of 10%) [9], primarily due to incomplete information from nuclear databases. On the other hand, for ^{235}U , ^{239}Pu , ^{241}Pu , $\bar{\nu}_e$ energy spectra have been derived from measured electron spectra at ILL, with an average uncertainties less than 2%, mainly originated from the uncertainty due to the conversion from electron to neutrino spectra [18]. For ^{238}U (fast neutron-induced fissions), only theoretical calculations exist at present [9, 19]. The isotopic concentration in fuel evolves with reactor operation time, so does the fission rate of each isotope. To predict neutrino flux

at a given time, commercial reactor in particular, detailed core simulation is needed, which carries its own uncertainty. For research reactors like CARR, however, ^{235}U enrichment is much higher than that of commercial reactors, fissions of which dominate the total fission rate. For simplicity, we shall ignore burnup effects and assume a pure ^{235}U neutrino spectrum for CARR in the remainder of this work. The difference in shape between a real and a pure ^{235}U will be considered as a shape uncertainty (bin-to-bin).

In this work, we adopted the simple parameterization in [20] for ^{235}U neutrino energy spectrum,

$$f(E_\nu) = e^{0.870 - 0.160E_\nu - 0.0910E_\nu^2}, \quad (1)$$

in units of $\bar{\nu}_e/(\text{MeV} \cdot \text{fission})$, also shown in Fig. 1.

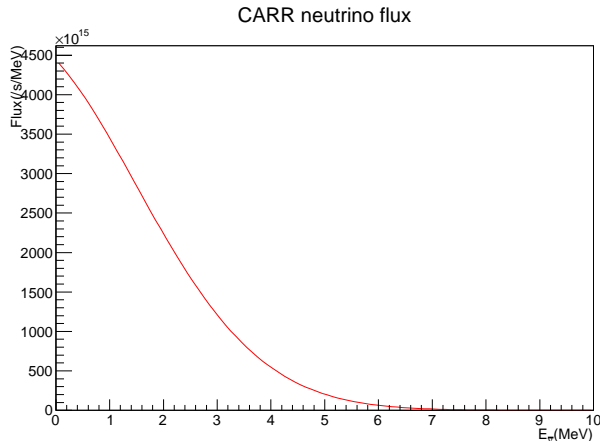


FIG. 1: Emitted neutrino flux ($/\text{s}/\text{MeV}$) at CARR assuming pure ^{235}U fissions with the parameterization given in [20].

The energy release per fission for ^{235}U is 201.7 ± 0.6 MeV in [21] and 201.92 ± 0.46 MeV in [22]. We take an average with $E_{re} = 201.8$ MeV. For CARR ($P_{th} = 60$ MW), the expected neutrino spectrum emitted from the core per unit time is:

$$F(E_\nu) = \frac{P_{th}}{E_{re}} \cdot f(E_\nu). \quad (2)$$

III. $\bar{\nu}_e$ DETECTION

Neutrino-target interaction cross section is low, typically of the order of 10^{-44} cm^2 . Background suppression is a key consideration of such experiments. On the other hand, short

baseline requirement and space constraint dictate that the neutrino detector has to be placed above ground without large shielding structure. To suppress background, we investigated three detection techniques, all with timing coincidence signatures.

A. Inverse- β decay with liquid scintillator

The classical method for detecting reactor $\bar{\nu}_e$ is the so-called inverse- β decay (IBD),

$$\bar{\nu}_e + p \rightarrow e^+ + n. \quad (3)$$

Liquid scintillator (LS), usually with $>10\%$ hydrogen in mass (11% assumed in this study), is commonly used both as the target and detector for this reaction. The positron loses kinetic energy immediately and annihilates into two 511 keV gammas, emitting prompt scintillation lights. The neutron will undergo thermalization collisions with hydrogen, and eventually get captured, emitting gamma rays which are converted into delayed scintillation lights. The neutrino energy can be reconstructed via $E_{e^+} \simeq E_\nu - 1.8$ MeV, where E_{e^+} and E_ν are the kinetic energy of the positron and neutrino, respectively. The detected prompt energy E_p , on the other hand, contains both the positron kinetic energy as well as the annihilation energy, i.e. $E_p = E_{e^+} + 1.022$ MeV. To enhance neutron detection efficiency and suppress background, most modern experiments adopt Gadolinium-doped LS (GdLS) – the ~ 8 MeV n-Gd capture gamma rays can be used as a clean neutron tag.

Taking into account higher order electroweak corrections, the cross section of the IBD is given in [23]. Folding it with reaction neutrino spectrum (Eqn. 2), detected neutrino spectrum (without oscillation) can be written as

$$N_{no-osc}(E_\nu) = \frac{N_p}{4\pi L^2} \epsilon(E_\nu) F(E_\nu) \times \sigma_{IBD}(E_\nu) \times T, \quad (4)$$

where N_p is the number of target protons, $\epsilon(E_\nu)$ is the detector efficiency, and T is the duration of the measurement. The resulting neutrino spectrum is shown in Fig. 2, where the 1.8 MeV reactor threshold of the IBD is manifest in the curve. To set the scale, the average detected neutrino rate (assuming 100% detection efficiency) is about 7000/MW/ton/year at 7 m. The oscillated neutrino rate and spectrum will deviate from this spectrum for a given set of oscillation parameters, as illustrated in Fig. 2.

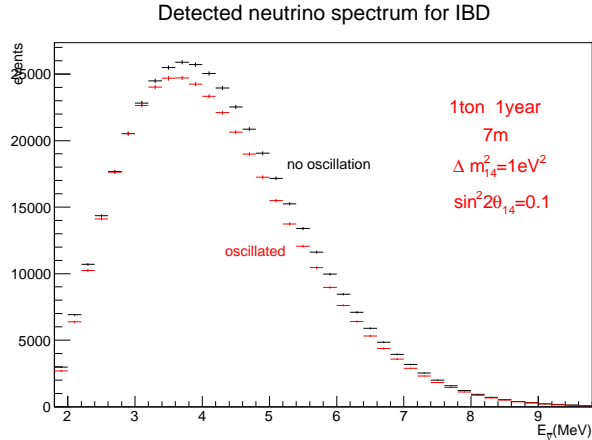


FIG. 2: Measured IBD neutrino spectrum without (black) and with (red) oscillation. Uncertainties are statistical only.

B. IBD with light water

A common background for IBD detection with LS is the fast neutron background. The recoiling protons created by a fast neutron will scintillate and mimic the prompt energy from the IBD before the neutron get captured. Since CARR is a surface facility, fast neutrons background induced by cosmic muons and from the reactor itself may pose serious challenge to the experiment.

To mitigate this, if the target is water instead of scintillator, recoiling protons would not be able to make Čerenkov lights, therefore get rejected. The technology of Gadolinium-doping in water was proposed in 2004 [24] and has been under active development [25], so it would be possible to maintain this clean neutron capture tag. However to use this approach in reactor neutrino experiment there are two obvious challenges:

1. The amount of Čerenkov photons is much smaller compared to the scintillating photons. As a result, water detector has much worse intrinsic energy resolution compared to that of LS. We would have to increase the photocathode coverage to get a reasonable amount of photoelectrons (PEs).
2. The Čerenkov threshold for water is about 289 keV (positron kinetic energy). The (nonlinear) reconstruction from the visible Čerenkov lights to true neutrino energy will be quite different from the LS case.

A realistic estimate of the Čerenkov light yield is needed to address the first concern. Light yields for large water detectors are summarized in [1] with a range between 3-9 PE/MeV. Small detectors with less light attenuation and more reflections could end up with more lights. To test this, we performed a bench test using tagged cosmic ray impinging on an acrylic ball with 5 cm diameter containing pure water. The Čerenkov lights are viewed by four Hamamatsu R7725 photomultipliers close-by. The measured PE spectrum is shown in Fig. 3. The minimum ionization bump (~ 8 MeV) is located at ~ 33 PE. If we extrapolate this result (photocathode coverage of $\sim 12\%$) to an experiment with $>50\%$ coverage, a light yield of 16 PE/MeV energy deposition would be attainable. The energy resolution would still be quite low compared to the LS, but it appears that a 30% resolution would be achievable at 1 MeV.

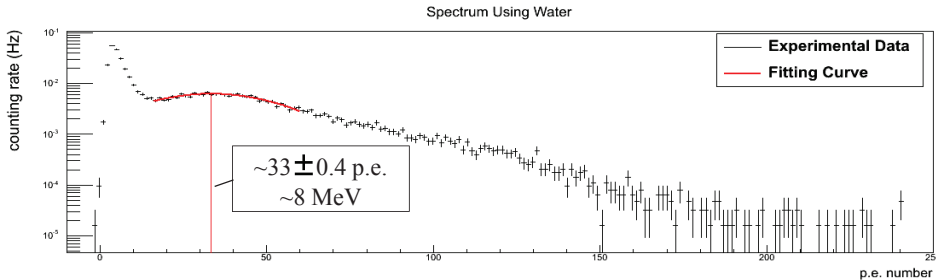


FIG. 3: Measured muon photoelectron spectrum with a prototype water detector. The solid angle coverage by photocathode is $\sim 12\%$.

The second concern can only be addressed through comprehensive calibration. Not only one needs a careful calibration with gamma sources, but also electron sources (beta or conversion electrons) or positron sources to establish the energy nonlinearity. The elaborated calibration programs developed at SuperK [26] and SNO [27] provide invaluable guidance in this regard.

C. $\bar{\nu}$ -D with heavy water

Room gamma background, when in accidental coincidence with random (cosmic or reactor) neutron capture signals, can form IBD-like background. If such background is significant compared to the IBD signals, it may become a serious issue (although in principle such a background can be statistically subtracted).

To further suppress background, we have considered heavy water (D₂O) as a potential target. In 70's of the last century, Reines *et al.* pioneered ν -D measurements at nuclear reactors [28]. Reactor $\bar{\nu}_e$ s are detected via $\bar{\nu}_e$ -deuteron charge current scattering:

$$\bar{\nu}_e + D \rightarrow n + n + e^+ \quad (5)$$

with the total kinetic energy of the positron given by

$$E_{e^+} \simeq E_\nu - 4\text{MeV} \quad (6)$$

The detection signal now becomes a triple coincidence between the prompt positron signal and two delayed neutron capture signals. Neutron captures on deuteron will give a single 6.25 MeV gamma ray. To avoid energy leakage for this high energy gamma, one could dope the heavy water with salt (NaCl) so that neutron capture on Chlorine gives a total energy of ~ 8.6 MeV, distributed in 2 or 3 gamma rays [29]. The signals produced by fast neutron will be singles, the same as in a water detector. Accidental backgrounds will be highly suppressed by the triple-coincidence requirement. It should be noted that $\bar{\nu}_e$ can also scatter off from D via neutral current channel, $\bar{\nu}_e + D \rightarrow n + p + \bar{\nu}_e$, but with no coincidence signature.

A tabulated charge-current $\bar{\nu}_e$ D cross section can be found in [30]. The measured spectrum with no oscillations is now

$$N_{\text{no-osc}}(E_\nu) = \frac{N_D}{4\pi L^2} \epsilon(E_\nu) F(E_\nu) \times \sigma_{\nu-D}(E_\nu) \times T. \quad (7)$$

With a lower cross section and higher energy threshold, the total number of detected neutrino events at 7 m is about 92/year/MW/ton (100% detection efficiency), 2 orders of magnitude less than that of IBD. Illustrated in Fig. 4 is a comparison of a non-oscillation and oscillated spectrum. One should emphasize that the main advantage of D₂O is its unique ν -D charge current signature which may lead to a background-free measurement.

For reference, number of detected neutrino events at CARR using three different targets (1 ton·1 year·100% efficiency) at 7 m are tabulated in Table I.

IV. BACKGROUND ESTIMATION

Direct determination of reactor-on background in the CARR experimental hall has yet to be performed, awaiting for the operation of the reactor. In this section, background estimation will be given based on current best knowledge at CARR and projections from other experiments, serving as a rough guidance to the design of the experiment.

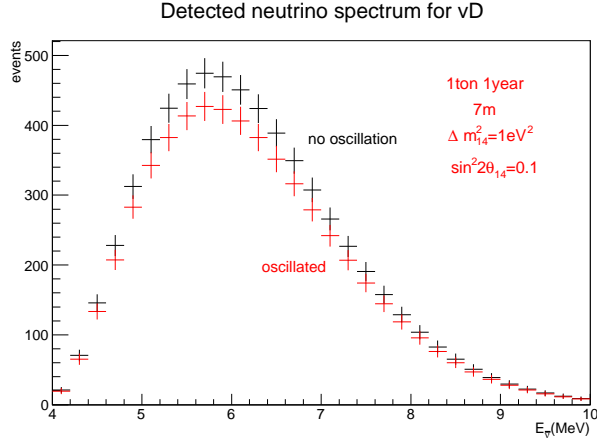


FIG. 4: Measured ν -D charge current spectrum without (black) and with (red) oscillation. Error bars are statistical only for a 1-ton target at 7 m operating for a year.

Target	Liquid scintillator	H ₂ O	D ₂ O
Non-osc (/ton/year)	420129	369505	5515
Osc (/ton/year)	394667	345329	4998

TABLE I: Event rate at 7 m with 100% efficiency. Non-osc: $\sin^2 2\theta_{14}=0$; Osc: $\Delta m_{14}^2 = 1 \text{ eV}^2$, $\sin^2 2\theta_{14}=0.1$.

A. Trigger rate

Gamma rays (external and internal) and cosmic muons are two major contributors to the detector raw trigger rate.

We have not made dedicated gamma spectrum measurement at CARR, but earlier commissioning run indicated that the dose rate was less than $3 \mu\text{Sv/h}$, which translate to an upper limit of gamma flux of 150 Hz/cm^2 , or $<\sim 7.5 \text{ MHz}$ for a ton-scale detector. With a 20 cm of Pb shielding backed up by 5 cm of pure cooper, the external gamma rate can be cut down to $<10 \text{ Hz}$ ($>1 \text{ MeV}$ threshold). The internal gamma background can only be suppressed by careful material screening and selection. For reference, the internal background contributes to $<70 \text{ Hz}$ (0.7 MeV threshold) to the trigger rate of Daya Bay detector (20 ton). If we assume similar materials (stainless steel tank, acrylic vessel, etc), similar phototube coverage, and same GdLS in a ton-scale detector, the internal background would contribute to $<10 \text{ Hz}$ for the 1 MeV threshold.

The integral intensity of vertical muons at the sea level is about $60\text{m}^{-2}\text{s}^{-1}\text{sr}^{-1}$ [1]. The total area of the ton-scale detector seen by muons from all directions is estimated to be 2m^2 , leading to a trigger rate of at least 120 Hz. Muon-induced backgrounds and possible photomultiplier afterpulsing will also contribute to the trigger rate.

Conservatively, we estimate a raw trigger rate of <500 Hz, which can be comfortably handled by commercial electronics.

B. Time-correlated background rate

As mentioned above, background in $\bar{\nu}$ -D charge current channel is hugely suppressed by the triple coincidence requirement. Here we focus on the time-correlated background in the IBD channel. We divide the background into two categories: reactor-associated and reactor-independent. They can be further sub-divided into correlated and accidental background.

1. reactor-associated background

On average, each fission produces 2-3 fission neutrons [31]. Thus for a 60MW_{th} reactor, the total fission neutron flux from the core is estimate to be $5 \times 10^{18}/\text{s}$. Most of reactor-associated background is due to neutrons from the reactor core as well as secondary gammas from neutron capture on metal or concrete surrounding the core. Since CARR is a neutron scattering facility with many neutron guides from the core, it is difficult to accurately estimate the neutron background at the detector location. As a start, we assumed an ideal spherical geometry and used a GEANT4-based toy Monte Carlo program to transport fission neutrons from the core through heavy water (1 m), water (1.65 m), and concrete shielding wall (2.1 m). The neutron spectrum emitting from the concrete wall is shown in Fig. 5 together with initial fission neutrons spectrum. The shielding factor for neutrons above 1 MeV is calculated to be 3.8×10^{19} under this geometry. About one third of these residual fast neutrons carry a kinetic energy >4 MeV (corresponding to a prompt visible energy >1 MeV). So without any neutron shielding around the detector, and taking into account the detector acceptance ($\sim 2 \times 10^{-3}$ at 7 m), we estimate a correlated rate of $< 1 \times 10^{-4}/\text{s}$, two order of magnitude lower than the IBD signal [42]. Pulse shape discrimination is reported to be able to distinguish nuclear recoil from electron recoil signals in LS [32, 33]. This could

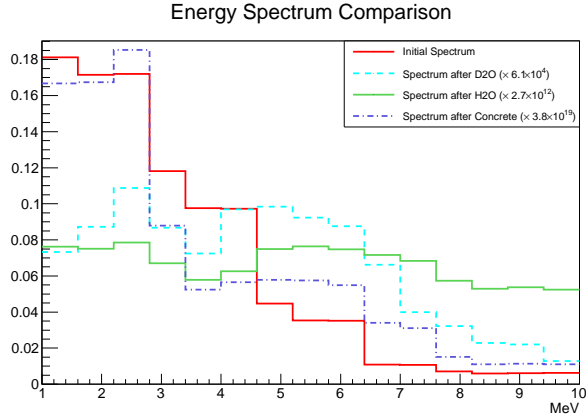


FIG. 5: Energy spectrum for the residual reactor fast neutron background predicted by a GEANT4 Monte Carlo.

lead to another powerful background suppression factor.

As mentioned earlier, fast neutron background is absent in the water and heavy water detectors. In all three detectors, slow neutrons will only make a single capture signal, contributing to accidental background only. Our high energy threshold on the delay-like events remove most gamma background from the natural radioactivity, but not single neutrons that captured in the target via n -Gd (LS or water) or n -Cl (heavy water) or high energy gamma rays caused by neutron captured on environmental metal materials (Fe/Cr/Ni etc.) [34]. It is difficult to estimate delay-like background without direct reactor-on measurement. Just for reference, the NUCIFIER experiment [43] estimated that such a background contribute to B/S of 1:1 for their IBDs [34] with 10 cm of Pb shielding. A 20 cm Pb shielding at CARR may further suppress this background.

It is interesting to note that other experiments at research reactors also have measured reactor-correlated background. For example, the ILL reactor neutrino experiment reported no such background [35].

2. reactor-independent background

As the detector is placed at the surface, the reactor-independent background is dominated by neutrons created by cosmic muons (LS detector). Muons can be separated in two categories: a) “LS muons” with long trajectories in the LS so the detector itself has 100% tagging efficiency, b) “corner muons” with short or no trajectory in the LS therefore missed

by the detector. Fast neutrons produced by corner muons will be untagged, producing dangerous background to the experiment.

To suppress untagged neutron background, we assume a simple outer muon veto system, e.g. two layers of plastic scintillator paddles, with an efficiency 95%. Let us further assume that the paddles cover an area of 4 m² on the surrounding dead materials or corners which would have been missed by a bare LS detector. For an area of 4 m², the muon rate is estimated to be 60 × 4 = 240 Hz. If we veto all IBD-like candidate within 200 μs to a muon detected by the paddles [2], additional deadtime introduced to the experiment is only 4.8%.

The residual fast neutron background in the detector after the paddle veto is estimated using empirical parameterization in [36]

$$N_n = 4.14E_\mu^{0.74} \times 10^{-6}/(\mu \cdot \text{g}/\text{cm}^2). \quad (8)$$

where E_μ is the muon energy in GeV. Let us conservatively assume that the 5% unvetoes muons each have an effective path length of 100 g/cm² in the detector (although they only hit the dead surrounding material), we get an untagged spallation neutron rate of

$$240 \times 5\% \times 4.14 \times 4^{0.74} \times 10^{-6} \times 100 \sim 0.01\text{Hz}$$

where surface muon average energy $\langle E_\mu \rangle \sim 4$ GeV [1] has been assumed. This background is comparable to the IBD signal rate. Other background due to muons hitting outside the 4 m² area is expected to be small.

Cosmic ray induced fast neutrons in the LS can be further suppressed via following handles. First, neutron tagging efficiency can be improved by employing more layers of muon paddles. Second, as illustrated in [37], a model independent way to remove all reactor-independent background is to use the “reactor on–off”. Third, as mentioned in Sec. IV B 1, pulse-shape discrimination technique may help to veto neutron recoil signals. For water and heavy water detectors, on the other hand, there is no correlated background of this nature.

Muon spallation on carbon in the liquid scintillator will produce beta-delayed neutron emitters ⁹Li or ⁸He, two classical correlated background (β =prompt, n =delayed) for the liquid scintillator-based experiments. Due to the long half-live (0.18 and 0.12 s), one can not tag them with parent muons nor is it practical to veto all muons for a long \sim s time window. If we extrapolate from the fitted results at Daya Bay near site: \sim 30/day/20-ton for an average muon energy of 55 GeV and rate of 20 Hz [38], we get a surface rate

of 1.3/day/ton assuming that the production yield shares the same $E_\mu^{0.74}$ dependence as the neutrons. This background is negligible compared to the IBD rate, and again, can be subtracted by reactor-off data.

V. SENSITIVITY TO STERILE NEUTRINO SEARCH

In what follows, we investigate the sensitivity of these neutrino detector to potential anti-electron to sterile neutrino oscillations. For simplicity, we shall dwell in the 3(active)+1(sterile) framework. At short distance(<15 m) from the reactor, the oscillation from standard 3×3 mixing parameters can be neglected, so the electron anti-neutrino's survival probability is

$$P_{ee} = 1 - \sin^2 2\theta_{14} \sin^2\left(1.27 \frac{L}{E_\nu} \Delta m_{14}^2\right) \quad (9)$$

in which L is the baseline (distance from reactor core to detector) in meter, E is the neutrino energy in MeV, and Δm_{14}^2 is the mass square difference between ν_4 and ν_1 mass eigenstates in eV^2 . Taking into account the oscillation, the detected neutrino spectrum for a perfect detector (Eqn. 4, 7) is modified into

$$N_{osc}(E_\nu) = P_{ee} N_{no-osc}(E_\nu) \quad (10)$$

In the reminder of this note, we assume a 60 MW_{th} reactor, 1 year running time, 1 ton fiducial mass, and 100% detection efficiency as the default exposure. Results for different exposure can be projected straightforwardly.

A. Detector Response Function

As mentioned in Sec. III A and III C, the positron kinetic energy E_{e^+} is simply related to neutrino energy E_ν . On the other hand, the detectable prompt energy of the three media is different. For LS, as mentioned in Sec. III A, we have $E_p = E_{e^+} + 1.022$ MeV. For water and heavy water detector, due to the Čerenkov threshold, the annihilation energy is hardly visible, so $E_p = E_{e^+}$. To get realistic visible energy spectrum, we convolve E_p with a simple Gaussian smearing (resolution) and a step-wise threshold function, so

$$N_{vis}(E_{vis}) = \mathcal{T}(E_{vis}) \int N(E_p) \mathcal{G}(E_{vis} - E_p) dE_p. \quad (11)$$

In this expression, $\mathcal{G}(E_{vis} - E_p)$ is Gaussian with a width of $10\%/\sqrt{E_p}$ for liquid scintillator, and $30\%/\sqrt{E_p}$ for water and heavy water (Sec. III B), and

$$\begin{aligned} \mathcal{T}(E_{vis}) &= 1 \text{ LS} \\ &= 1(E_{vis} > 1\text{MeV}) \\ &= 0(E_{vis} < 1\text{MeV}) \end{aligned} \left. \vphantom{\begin{aligned} \mathcal{T}(E_{vis}) \\ = 1(E_{vis} > 1\text{MeV}) \\ = 0(E_{vis} < 1\text{MeV}) \end{aligned}} \right\} \text{water and heavy water.} \quad (12)$$

$N(E_p)$ is the prompt energy spectrum assuming a perfect detector, i.e. N_{no-osc} in Eqn. 4 or 7 for no oscillation hypothesis, or N_{osc} in Eqn. 10 when disappearance is taken into account.

B. χ^2 Definition

The sensitivity of an given experimental setup to a given set of oscillation parameter $(\sin^2 2\theta_{14}, \Delta m_{14}^2)$, in short, is the power that one could differentiate the measured spectrum from a non-oscillation spectrum. Typically one defines a χ^2 function as the measure of such difference. In this application, it should satisfy that 1) $\chi^2 = 0$ when $\theta_{14} = 0$, 2) for a given value of Δm_{14}^2 , its variation w.r.t. $\sin^2 2\theta_{14}$ follows the standard χ^2 distribution. Then to determine the exclusion limit to a given confidence integral (e.g. 95.5%), for each given Δm_{14}^2 we would scan over the value of $\sin^2 2\theta_{14}$ to generate measured spectrum, and determine the boundary of the corresponding χ^2 (e.g. $\chi^2 = 4$).

Omitting background related systematics [44], the χ^2 can be defined as [39]

$$\begin{aligned} \chi^2 = \sum_{i=1, nbins} & \frac{[N_{vis,osc}^i - N_{vis,no-osc}^i \cdot (1 + \alpha + \frac{(L+\gamma)^2}{L^2} + f^i(\eta, \beta))]^2}{N_{vis,osc}^i [1 + \sigma_{b2b}^2 N_{vis,osc}^i]} \\ & + (\frac{\alpha}{\sigma_{norm}})^2 + (\frac{\eta}{\sigma_{eshift}})^2 + (\frac{\beta}{\sigma_{escale}})^2 + (\frac{\gamma}{\sigma_L})^2. \end{aligned} \quad (13)$$

where $N_{vis,osc}^i$ and $N_{vis,no-osc}^i$, respectively, represent the i th energy bin in the visible energy spectrum (Eqn. 11) with and without oscillation. This is so-called ‘‘rate+shape’’ χ^2 . The following systematics have been considered (see also Table II): 1) a 3% normalization uncertainty σ_{norm} (including reactor total neutrino flux, target protons, and detector efficiency) and its nuisance parameter α ; 2) energy non-linearity including a shift σ_{eshift} (0.02 MeV) and a scale factor σ_{escale} (1%), and their corresponding nuisance parameters η and β ; 3) 2% bin-to-bin uncorrelated shape uncertainties σ_{b2b} , which is added to the denominator of the first term for simplicity instead of introducing N_{bins} of pull terms; $f^i(\eta, \beta)$ represents

fractional change of counts in bin i for a given set of parameter (η, β) away from $(0,0)$; 4) a 10 cm position accuracy of the center of the core σ_L , conservatively being assumed to be along the radial direction, and the corresponding nuisance parameter γ [45]. The effects of detector resolution and threshold have been included automatically by using detected $N_{vis,osc}^i(E_{vis})$ and $N_{vis,non-osc}^i(E_{vis})$ (see Eqn. 12) in Eqn. 13. If one wants to perform a “rate-only” analysis, it is equivalent to using the above χ^2 with a single visible energy bin and set η , β , and σ_{b2b} to zero.

The impact of reactor flux can be further suppressed if we choose to use two identical detectors located at two different baselines, similar to the setup in the Daya Bay and RENO experiments [2, 3]. An earlier independent exploration on this approach can be found in [40]. In this case the χ^2 can be redefined as

$$\chi^2 = \sum_{d=n,f; i=1, nbin} \frac{[N_{vis,osc}^{d,i} - N_{vis,no-osc}^{d,i} \cdot (1 + \alpha + \epsilon^d + \frac{(L^d + \gamma)^2}{(L^d)^2} + f^i(\eta^d, \beta^d))]^2}{N_{vis,osc}^{d,i} [1 + \sigma_{b2b}^2 N_{vis,osc}^{d,i}]} \quad (14)$$

$$+ (\frac{\alpha}{\sigma_{norm}})^2 + (\frac{\gamma}{\sigma_L})^2 + \sum_d [(\frac{\epsilon^d}{\sigma_{eff}})^2 + (\frac{\eta^d}{\sigma_{eshift}})^2 + (\frac{\beta^d}{\sigma_{escale}})^2],$$

in which the superscript d runs between “near” and “far” to represent different quantities for the two detectors. We have also added a detector uncorrelated efficiency uncertainty σ_{eff}^d (0.5%) and its corresponding nuisance parameter ϵ^d . A summary of systematic components, the values, as well as whether they are correlated between the two detectors is given in Table II.

One should note that a couple of conservative approximations have been made in Eqn. 14. First, instead of introducing $nbins$ nuisance parameters for the bin-to-bin shape uncertainties, we assumed that these uncertainties are also uncorrelated between the near and far detectors, and lump them to the denominator of the first term just like the statistical uncertainties. Second, we have omitted detector correlated energy shift and stretch, and have assume η^d, β^d as detector uncorrelated nonlinearity. Both approximations have been verified to have negligible impact to θ_{14} sensitivity results.

C. Baseline optimization

Reactor neutrinos have a energy spectrum ranged up to 9 MeV, as shown in Fig. 1. The IBD ($\bar{\nu}$ -D) neutrinos has a energy peak at $E_\nu \simeq 3.7(5.7)$ MeV. If the true Δm_{14}^2 is around

Systematic uncertainty	Value assumed	Nuisance parameter	Near-Far Correlated
Overall normalization σ_{norm}	3%	α	C
Detector relative efficiency σ_{eff}	0.5%	ϵ^d	U
Energy shift σ_{eshift}	0.02 MeV	η^d	U
Energy scale σ_{escale}	1%	β^d	U
Reactor spectrum shape σ_{b2b}	2%	-	U
Baseline σ_L	10 cm	γ	C

TABLE II: Summary of systematic effects included in the two-detector χ^2 function in Eqn. 14. The last column indicates whether the component is correlated between the detectors: C=correlated, U=uncorrelated. Same systematic uncertainties are assumed for single-detector χ^2 (Eqn. 13) except for the detector efficiency, which we have absorbed into the normalization uncertainty.

1 eV², as implied by the global analysis, naively one would put the detector close to the first oscillation maximum to maximize the analyzing power, i.e. $L_{osc} = \frac{\pi}{2} \frac{E_\nu}{1.27\Delta m_{14}^2}$, translating into 4.6 (7.0) m for IBD and $\bar{\nu}$ -D CC neutrinos.

However, the above discussion is incomplete since we have omitted influence from statistics. The fact that the event rate is inversely proportional to L^2 makes the optimal baseline deviates from the naive oscillation maximum.

A more elaborated analysis was made by employing the χ^2 definition from Sec. V B. We assumed a fix parameter pair ($\sin^2(2\theta_{14}) = 0.1$ and $\Delta m_{14}^2 = 1$ eV²), and our later conclusion does not change significantly with the value of $\sin^2(2\theta_{14})$. Energy thresholds in Eqn. 12 have been assumed, but for simplicity we assumed no energy smearing and set nuisance parameters for energy nonlinearity (η, β), baseline uncertainty (γ), and the bin-to-bin uncertainty σ_{b2b} in Eqn. 13 to zeros. The optimal baseline was determined by scanning through baseline to find the maximum of χ^2 . In Fig. 6, the value of χ^2 vs. baseline is shown for all three type of detectors with a “rate-only” or “rate+shape” analysis. Outside the 5-m shielding wall from the core, coincidentally we observe that 7 meter is sufficiently close to the best baseline for all three detection methods either in “rate+shape” or “rate only” analysis. χ^2 map for different values of baseline and Δm_{14}^2 have also been shown in Fig. 7. One observes a general trend that the sensitivity for larger value of Δm_{14}^2 increases with decreasing far detector baseline, which is expected from the $L\Delta m^2/E$ dependence of the shape.

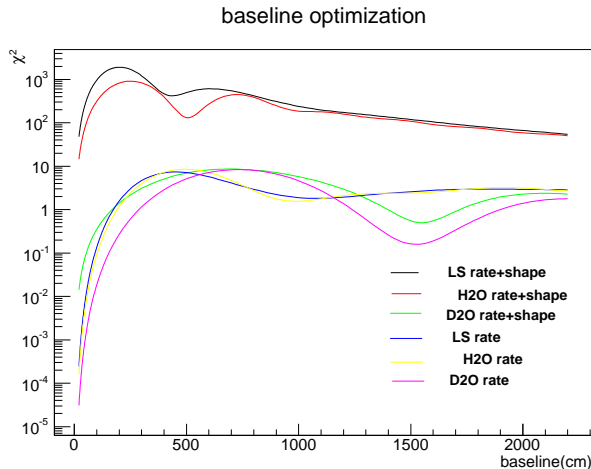


FIG. 6: Baseline optimization for single detector in “rate only” and “rate+shape” analyses for LS, light water and heavy water, with $\Delta m_{14}^2 = 1 \text{ eV}^2$ and $\sin^2 2\theta_{14} = 0.1$. See text for details.

For the two-detector scenario, since 7 m is approximately the closest distance that we can put the detector, we settle the near detector at this baseline. To determine the optimal baseline for the far detector, instead of using the two-detector χ^2 in Eqn. 14 (in which one still has to input the expected “non-osc” reactor spectrum), we adopted an approach to construct a pure relative measurement. We used the one-detector χ^2 in Eqn. 13, and demanded that $N_{vis,no-osc}^i = \frac{(L^n)^2}{(L^f)^2} N_{vis,osc}^{n,i}$, a scaled near detector spectrum. In general, this approach does not give the best sensitivity as it entirely omits the theoretical knowledge on reactor neutrino spectrum. On the other hand, the systematic uncertainty due to theoretical assumption is also completely avoided. The results of the baseline scan under this approach are shown in Fig. 8). The best far detector baseline is about 11 m for both LS and water in “rate+shape” analysis, and about 9 m for LS and 10 m for water in “rate only” analysis. The optimal baseline for heavy water is about 14 m for both analyses. For two-detector discussions in the rest of this paper, we will assume the optimal baselines in “rate+shape” analyses, i.e. a near detector at 7 m, and a far detector at 11 m (LS & water) or 14 m (heavy water) [46].

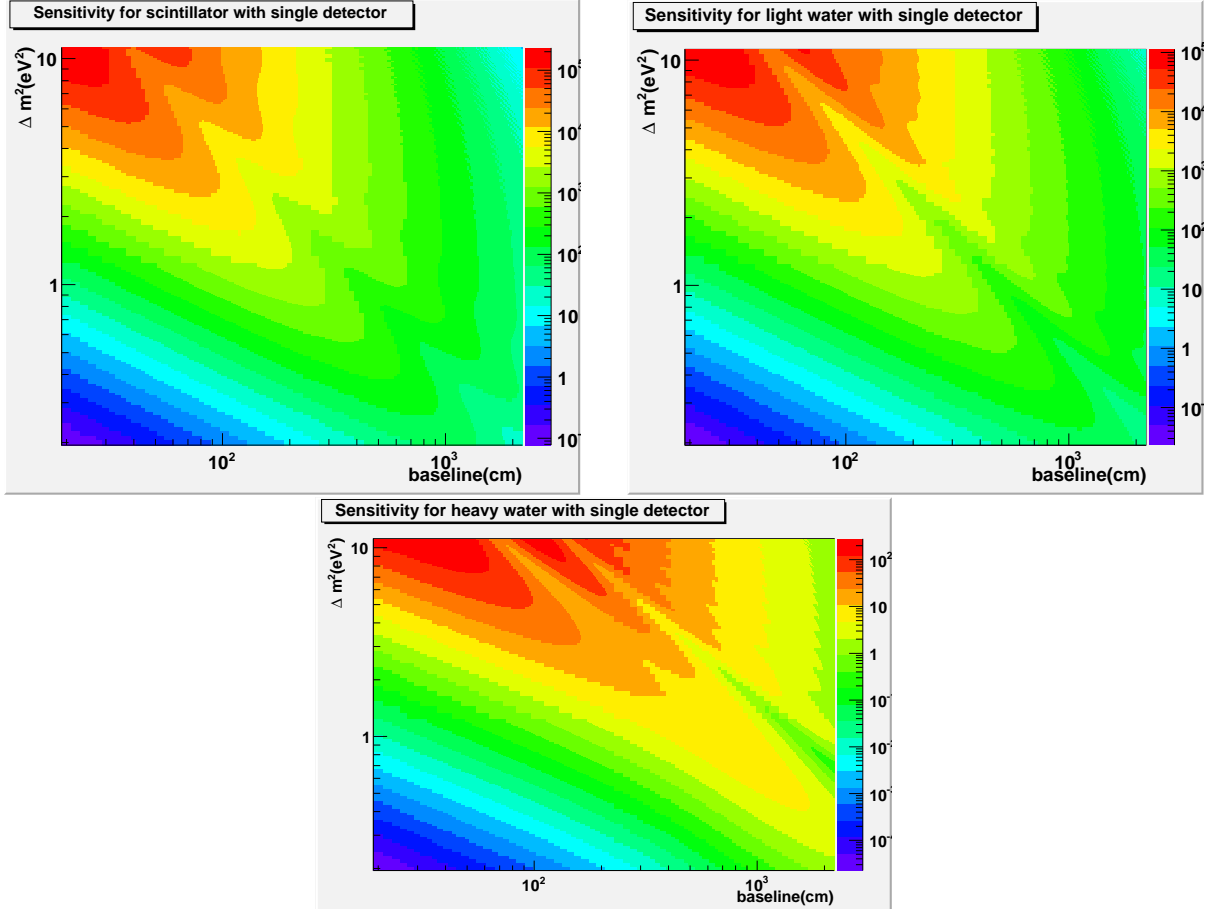


FIG. 7: χ^2 map vs. baseline and Δm_{14}^2 for LS (top left), light water (top right) and heavy water (bottom) in “rate+shape” analysis. 3% normalization uncertainties has been considered in the χ^2 calculation, but not other systematic uncertainties.

D. Sensitivity results

1. Single detector

Using the full χ^2 definition in Eqn. 13, the 95.5% exclusion curves for the three detection methods are shown in Fig. 9 in the $(\sin^2 2\theta_{14}, \Delta m_{14}^2)$ plane.

With “rate-only” analysis, we observe that for all three techniques, the 2σ sensitivity limits are around 0.1 even at optimum Δm_{14}^2 , due to the large normalization uncertainty. The sensitivity curves for LS and light water track with each other, although the latter is slightly worse due to a larger detection threshold. Both experiments are most sensitive to $\Delta m_{14}^2 \simeq 0.65 \text{ eV}^2$. For Δm_{14}^2 larger than $\sim 3 \text{ eV}^2$, the oscillation as a function of energy

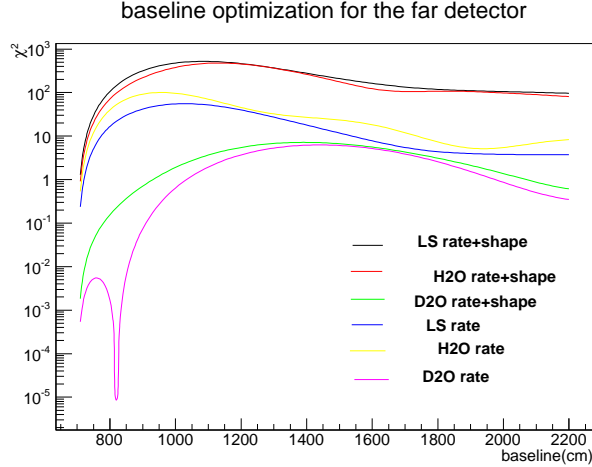


FIG. 8: Baseline optimization for far detector with the near one placed at 7 m from the core in “rate only” and “rate+shape” analyses for LS, light water and heavy water, with $\Delta m_{14}^2 = 1 \text{ eV}^2$ and $\sin^2 2\theta_{14} = 0.1$. See text for details.

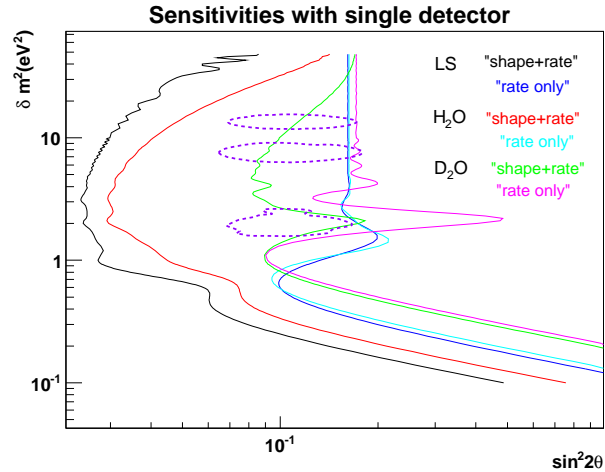


FIG. 9: Sensitivities for a single detector using LS, water and heavy water in “rate+shape” analysis. All systematics in Eqn. 13 have been considered. The dashed contours are the 68% confidence contours in [13] (only those with χ^2 local minima < 1 are selected to indicate global fits’ most favored parameter space and for visual clarity).

becomes so fast that it get smeared out by the energy resolution of the detector. In this case, one measures a constant deficit ($\propto 1/2 \sin^2(2\theta_{14})$) independent of the baseline, giving rise to a constant sensitivity at large Δm_{14}^2 . The heavy water sensitivity is not so much worse than the other two, as the dominating uncertainty comes from the normalization, not

the statistics. The value of Δm_{14}^2 where the best sensitivity occurs is ~ 1 eV², higher than that of the IBD, due to higher reaction threshold (~ 4 MeV) thereby higher average detected neutrino energy.

The situation is drastically improved with a “rate+shape” analysis. All three exclusion curves moved to much smaller value of $\sin^2 2\theta_{14}$ in Fig. 9, LS and water in particular, as the constraints from the shape will seriously combat the large normalization uncertainty. It is also interesting to note that the value of Δm_{14}^2 where experiments are most sensitive to has undergone significant changes compared to that in “rate-only” analysis. This can also be understood as an effect from the shape constraints. For example, for IBD, at $\Delta m_{14}^2 \simeq 0.65$ eV² the overall disappearance in rate is the largest (on top of the 3% uncertainty in normalization), but the shape distortion is flatter compared to say $\Delta m_{14}^2 = 1$. Therefore it would be relatively easier to choose a normalization nuisance parameter to balance the spectrum distortion. For heavy water, the “rate+shape” analysis helps, but not as much as the IBD, as a result of lower statistics in each energy bin.

2. Two detectors

The sensitivity with two detectors can be investigated in a similar way using the χ^2 in Eqn. 14. Conceptually, unlike the design of Daya Bay and RENO experiments [2, 3] (using well-known Δm^2), with an unknown Δm_{14}^2 the “rate-only” relative measurement becomes much dicier. For certain values of Δm^2 , the normalized event rates at near and far sites would equal to each other therefore would cancel the sensitivity in the near/far ratio. Under this “unlucky” situation, one could still gain some sensitivity back by relying on the flux prediction, but the main purpose of two-detector design would be largely undermined.

The story is drastically different once the detector shape information is used, due to the L/E dependence of oscillated spectrum. Within two-detector scenario, the sensitivity curves with “rate+shape” analysis are shown in Fig. 10 for LS, H₂O and D₂O. One clearly observes an improved sensitivity compared to Fig. 9 for all detectors. This is anticipated, since the χ^2 construction in Eqn. 14 has used information from both detectors as well as the flux prediction.

To study contribution from each systematic component, we compared the variation of the exclusion curve on $(\sin^2 2\theta_{14}, \Delta m_{14}^2)$ when “turning off” systematics one-by-one. The results

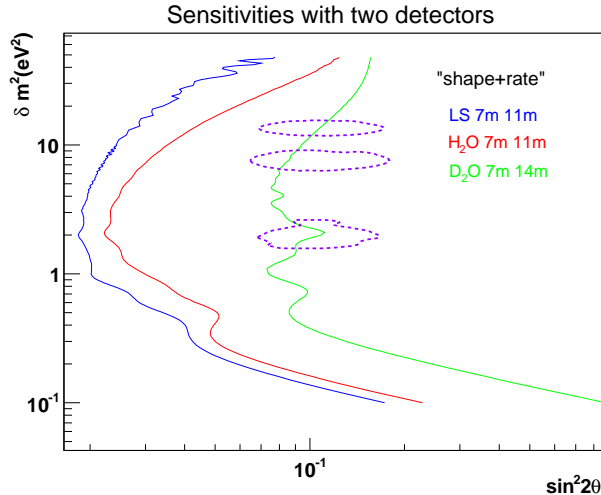


FIG. 10: Sensitivities for two identical detectors using LS, water and heavy water in “rate+shape” analysis. All systematics in Eqn. 14 have been considered. The dashed contours are the 68% confidence contours in [13] (only those with χ^2 local minima < 1 are selected to indicate global fits’ most favored parameter space and for visual clarity).

for the LS detector (most sensitive one) at $\Delta m_{14}^2 = 1 \text{ eV}^2$ is shown in Table III. Separated systematic uncertainties by taking the quadrature difference [47] are also tabulated in the table.

One sees that two-detector scheme not only improves the statistics, but also help to reduce the normalization uncertainty. The fact that the normalization uncertainty does not disappear completely is a result of the interplay between the rate and shape constraints. From experimental point of view, if detectors are constructed as movable, one could consider a “swap” between the near and far detectors in order to further suppress systematic uncertainties.

E. Effects due to energy and baseline smearing

The systematic effects discussed above can all be captured in individual nuisance parameters – if known to infinite precision, they will not lead to biases in neutrino rate or spectrum. Another class of systematics introduce smearing to the oscillation signals; one loses sensitivity no matter how accurately the smearing is known. Such effects cannot be easily incorporated as nuisance parameters in χ^2 , therefore require separate evaluation. In

Errors considered	Single detector	Two-detector
A+B+C+D+E+Stat.	0.02748	0.02017
A+B+C+D+Stat.	0.02701	0.01967
A+B+C+Stat.	0.02680	0.01934
A+B+Stat.	-	0.01746
A+Stat.	0.02321	0.01691
Stat. only	0.01055	0.00885

	Stat	Normalization	Efficiency	E stretch	E shift	Baseline
Single detector	0.011	0.021	-	0.013	0.004	0.005
Two-detector	0.009	0.014	0.004	0.008	0.004	0.004

TABLE III: Upper table: $2\text{-}\sigma$ sensitivity on $\sin^2 2\theta_{14}$ when adding in systematic effects one-by-one. Systematic uncertainties include: (A) normalization, (B) detection efficiency, (C) energy scale stretch, (D) energy scale shift, and (E) baseline uncertainty. The statistical and bin-to-bin shape uncertainties are always combined into a “stat” uncertainty. Target=LS. $\Delta m_{14}^2 = 1 \text{ eV}^2$. Single detector: 7 m. Two-detector: near @ 7 m, far @ 11 m. Lower table: breakdown of uncertainties by taking the quadrature differences from the upper table. The efficiency uncertainty for a single detector has been included into the normalization uncertainty.

this section, we discuss two major smearing effects: energy resolution and baseline smearing. The GdLS target is chosen in the study.

1. Energy resolution

To extract the impact of energy resolution to $\sin^2 2\theta_{14}$, we recalculated the sensitivity with perfect detector resolution (i.e. no energy smearing), and compare it to that with realistic energy resolution given in Sec. V A. Simply taking the quadrature difference, the contribution to $\sin^2 2\theta_{14}$ sensitivity at $\Delta m_{14}^2 = 1 \text{ eV}^2$ is less than $\sim 10^{-3}$ for both single and two-detector scenarios.

2. Baseline smearing

The distance $\bar{\nu}_e$ travels from its origin to IBD interaction point is smeared out due to finite-sized core and detector geometry. Several control rods are distributed in the core of CARR [41], therefore neutrino creation points can be approximated as uniform in a 40 cm diameter and 80 cm height cylinder. In Fig. 11 the baseline distribution for the near detector at 7 m is shown, assuming that the target region is a perfect cylinder with 1 m diameter and 1.5 m height. Obviously such distribution will cause a smearing to the L/E oscillation

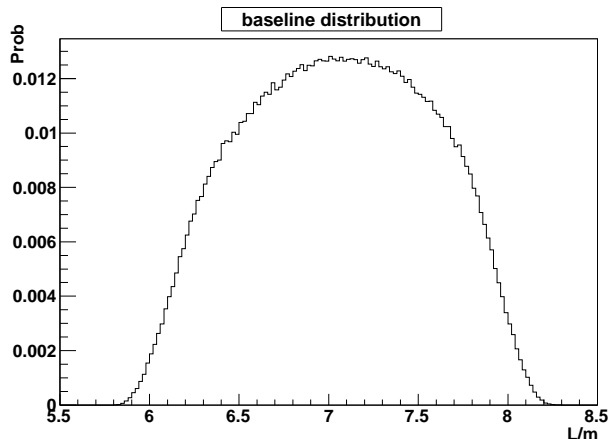


FIG. 11: Baseline distribution (PDF) for the near detector 7 m. See text for details.

signal. The contribution to $\sin^2 2\theta_{14}$ sensitivity was evaluated through the same quadrature difference procedure above. We obtain a loss of sensitivity of less than 2×10^{-3} in $\sin^2 2\theta_{14}$ for both the single detector and two-detector scenarios for $\Delta m_{14}^2 = 1 \text{ eV}^2$.

VI. DISCUSSION AND CONCLUSION

Under the framework of “3+1” neutrino mixing, we have conducted a study of the sensitivities to $\sin^2 2\theta_{14}$ at short baseline ($< 15\text{m}$) to a research reactor (CARR) using three targets (LS, H_2O , and D_2O). This study suggests that in the absence of background, the LS detector has the best sensitivity due to higher IBD reaction rate and more superior energy resolution. For an experiment detecting $\bar{\nu}$ -D CC scattering using heavy water, the event rate is far less, with a powerful suppression of potential background nevertheless. From the comparison between “rate-only” and “rate+shape” analyses, we conclude that the spectrum

distortion provide crucial handle to oscillation therefore a key to the experiment design. To cancel uncertainties from the reactor flux prediction, we compared the performance of a single-detector and two-detector design. The latter leads to not only a better sensitivity but also a suppression of systematic uncertainty. Under the current best scenario (liquid scintillator, two-detector, no background, and “rate+shape” analysis), a ton-scale detector operating for a year can reach a sensitivity (95.5%) of ~ 0.02 to $\sin^2 2\theta_{14}$ for $\Delta m_{14}^2 \sim 1 \text{ eV}^2$, severely constraining the sterile-to-regular oscillation parameter space suggested by global analysis.

VII. ACKNOWLEDGMENTS

This work was done with support from the Shuguang Foundation of Shanghai Grant Z1127941, and Shanghai Laboratory for Particle Physics and Cosmology at the Shanghai Jiao Tong University. The authors acknowledge Prof. Karsten Heeger from the Univ. of Wisconsin for an initial discussion on sterile neutrinos, and Profs. Weiping Liu and Dongfeng Chen from CIAE for introducing the CARR reactor to us. We also acknowledge Drs. Yufeng Li from IHEP and Bryce R Littlejohn from the Univ. of Cincinnati for helpful suggestions to the paper draft.

-
- [1] J. Beringer *et al.* (Particle Data Group), Phys. Rev. D86, 010001 (2012)
 - [2] F. P. An *et al.* (Daya Bay Collaboration), Phys. Rev. Lett. 108 171803 (2012)
 - [3] J. K. Ahn *et al.* (RENO Collaboration), Phys. Rev. Lett. 108, 191802 (2012).
 - [4] Y. Abe *et al.* (Double Chooz Collaboration), Phys. Rev. Lett. 108, 131801, Phys. Rev. D 86, 052008 (2012)
 - [5] P. Anselmann *et al.* (GALLEX. Collaboration), Phys. Lett. B 342 (1995) 440; W. Hampel *et al.* (GALLEX Collaboration), Phys. Lett. B 420, 114 (1998); F. Kaether, W. Hampel, G. Heusser, J. Kiko, and T. Kirsten, Phys. Lett. B 685, 47 (2010).
 - [6] D. Abdurashitov, V. Gavrin, S. Girin, V. Gorbachev, T. V. Ibragimova, *et al.*, Phys. Rev. Lett. 77, 4708 (1996); J. Abdurashitov *et al.* (SAGE Collaboration), Phys. Rev. C 59, 2246 (1999); J. Abdurashitov, V. Gavrin, S. Girin, V. Gorbachev, P. Gurkina, *et al.*, Phys. Rev.

- C 73, 045805 (2006); J. Abdurashitov *et al.* (SAGE Collaboration), Phys. Rev. C 80, 015807 (2009).
- [7] A. Aguilar *et al.*,(LSND Collaboration), Phys. Rev. D 64, 112007 (2001).
- [8] A. Aguilar-Arevalo *et al.* (MiniBooNE Collaboration), Phys. Rev. Lett. 102, 101802 (2009);
A. Aguilar-Arevalo *et al.* (MiniBooNE Collaboration), Phys. Rev. Lett. 105, 181801 (2010).
- [9] T. A. Mueller *et al.*, Phys. Rev. C 83, 054615 (2011);
- [10] P. Huber, Phys. Rev. C 84, 024617 (2011).
- [11] G. Mention, M. Fechner, T. Lasserre, T. Mueller, D. Lhuillier, *et al.*, Phys.Rev. D83, 073006 (2011).
- [12] C. Giunti and M. Lavede, Phys. Rev. D 84, 093006 (2011).
- [13] C. Giunti, M. Laveder, Y. F. Li, Q. Y. Liu, H. W. Long, Phys. Rev. D 86, 113014 (2013)
- [14] See, e.g., T.Asaka and M. Shaposhnikov, Phys. Lett. B 620, 17 (2005).
- [15] K. N. Abazajian et al, "Light Sterile Neutrinos: White Paper", arXiv:1204.5379, April 2012.
- [16] C. T. Ye, China Advanced Research Reactor (CARR): A New Reactor to be Built in China for Neutron Scattering Studies, Physica B 241-243, 48 (1998).
- [17] O. Yasuda, JHEP 1109:036 (2011).
- [18] K. Schreckenbach, G. Colvin and F. von Feilitzsch, Phys. Lett. B160, 325 (1985); F. von Feilitzsch and K. Schreckenbach, Phys. Lett. B118 (1982); A. A. Hahn *et al.*, Phys. Lett. B218, 365 (1989).
- [19] P. Vogel, G.K. Schenter, F.M. Mann and R.E. Schenter Phys. Rev. C 24, 1543 (1981); B. R. Davis, P. Vogel, F.M. Mann and R.E. Schenter, Phys. Rev. C19, 2259 (1979).
- [20] P. Vogel and J. Engel, Phys. Rev. D 39, 3378 (1989).
- [21] M. F. James, J. Nucl. Energy 23, 517 (1969).
- [22] V. Kopeikin *et al.*, Phys. Atom. Nucl., 67, 1892 (2004).
- [23] P. Vogel and J. F. Beacom, Phys. Rev. D 60, 053003 (1999).
- [24] J. F. Beacom and M. R. Vagins, Phys. Rev. Lett., 93, 171101 (2004)
- [25] Andrew Renshaw *et al.*, arXiv:1201.1017
- [26] Super-Kamiokande Collaboration, M. Nakahata *et al.*, Nucl. Instr. Meth. A421 113-129 (1999);
E. Blaufuss *et al.* Nucl. Instr. Meth. A 458, 636-647 (2001); F. Fukuda *et al.*, Nucl. Instrum. Meth. A501, 418-462 (2003).
- [27] SNO Collaboration, J. Boger *et al.*, Nucl. Instrum. Meth. A449 172-207 (2000); A. W. P. Poon

- et al.*, Nucl. Instr. Meth. A 452, 15-129 (2000); M. R. Dragowsky *et al.*, Nucl. Instr. Meth. A 481, 284-296 (2002); N. Tagg *et al.*, Nucl. Instr. Meth. A 489, 92-102 (2002); B. A. Moffat *et al.*, Nucl. Instr. Meth. A 554, 255-265 (2005); K. Boudjemline *et al.*, Nucl. Instr. Meth. A 620, 171-181 (2010).
- [28] E. Pasierb, H. S. Gurr, J. Lathrop, F. Reines and H. W. Sobel, Phys. Rev. Lett 43, 96 (1979).
- [29] B. Aharmim *et al.*, SNO Collaboration, Phys. Rev.C 72, 055502 (2005).
- [30] K. Kubodera and S. Nozawa, Int. J. Mod. Phys. E **3**, 101 (1994) [arXiv:nucl-th/9310014].
- [31] J. Cao, [arXiv:1101.2266 [hep-ex]]
- [32] H. O. Back *et al.* (Borexino Collaboration), Nucl. Instrum. Meth. A584, 98-113 (2008).
- [33] G. Ranucci, A. Goretti, P. Lombardi, Nucl. Instrum. Meth. A412, 374-386 (1998).
- [34] A. Porta *et al.* IEEE TRANSACTIONS ON NUCLEAR SCIENCE, VOL. 57, NO. 5, OCTOBER 2010.
- [35] H. Kwon *et al.*, Phys. Rev. D 24, 1097 (1981)
- [36] Y. F. Wang, V. Balic, G. Gratta, A. Fasso, S. Roesler and A. Ferrari, Phys. Rev. D 64, 013012 (2001).
- [37] F. Ardellier *et al.* (Double Chooz Collaboration), hep-ex/0606025 (2006)
- [38] F. P. An *et al.* (Daya Bay Collaboration), Chin. Phys. C 37, 80 (2013).
- [39] See, e.g., P. Huber, M Lindner, T. Schwetz, and W. Winter, Nucl. Phys. B665, 487 (2003)
- [40] K. M. Heeger, B. R. Littlejohn, H. P. Mumm and M. N. Tobin, Phys. Rev D 87, 073008, 2013
- [41] Wenxi Tian *et al.*, Ann. Nucl. Energ., vol. 34, no. 4, pp. 288296 (2007)
- [42] One should take this estimate under the caveat that the Monte Carlo had an oversimplified geometry. The real fast neutron background shall be directly measured.
- [43] Very similar core design as CARR.
- [44] Since we have no direct background measurement nor a shielding design yet, a particular choice of background would seem improper. We choose to present background-free scenario here, and instruct readers to bare this caveat in mind when reading the sensitivity curves.
- [45] In principle the γ term can be absorbed in the normalization uncertainty, but we leave them here to ease later discussion on two-detector sensitivity.
- [46] The final optimization of the far detector baseline will have to take into account the actual background levels. We also have to make the analysis choice of either an absolute measurement using reactor flux calculation, or a pure near/far relative non-null search. Here we only present

a particular choice of the far detector location to illustrate the advantage of two-detector scheme.

- [47] Although quadrature sum of these effects may not be strictly valid due to correlations, we take this approach to estimate the relative size of each component.